Recruitment of oriens-lacunosum-moleculare interneurons during hippocampal ripples

Maria Pangalos[a], José R. Donoso[b,c], Jochen Winterer[a], Aleksandar R. Zivkovic[a], Richard Kempter[b,c], Nikolaus Maier[a,1,2], and Dietmar Schmitz[a,c,d,e,1,2]

[a]Neurowissenschaftliches Forschungszentrum, Charité-Universitätsmedizin Berlin, 10117 Berlin, Germany; [b]Institute for Theoretical Biology, Humboldt-Universität zu Berlin, 10115 Berlin, Germany; [c]Bernstein Center for Computational Neuroscience, Humboldt-Universität zu Berlin, 10115 Berlin, Germany; [d]Cluster of Excellence NeuroCure, Charité – Universitätsmedizin Berlin, 10117 Berlin, Germany; and [e]Deutsches Zentrum für Neurodegenerative Erkrankungen in der Helmholtz-Gemeinschaft, Charité – Universitätsmedizin Berlin, 10117 Berlin, Germany

Edited* by Nancy J. Kopell, Boston University, Boston, MA, and approved January 29, 2013 (received for review September 6, 2012)

Sharp wave-associated ~200-Hz ripple oscillations in the hippocampus have been implicated in the consolidation of memories. However, knowledge on mechanisms underlying ripples is still scarce, in particular with respect to synaptic involvement of specific cell types. Here, we used cell-attached and whole-cell recordings in vitro to study activity of pyramidal cells and oriens-lacunosum-moleculare (O-LM) interneurons during ripples. O-LM cells received ripple-associated synaptic input that arrived delayed (3.3 ± 0.3 ms) with respect to the maximum amplitude of field ripples and was locked to the ascending phase of field oscillations (mean phase: 209 ± 6°). In line, O-LM cells episodically discharged late during ripples (~6.5 ms after the ripple maximum), and firing was phase-locked to field oscillations (mean phase: 219 ± 9°). Our data unveil recruitment of O-LM neurons during ripples, suggesting a previously uncharacterized role of this cell type during sharp wave-associated activity.

CA1 O-LM cell | CA1 pyramidal cell | sharp wave-ripples

Hippocampus-dependent memory consolidation is related to neuronal population rhythms. In particular, oscillations of the hippocampal local field potential (LFP) are associated with learning-induced network reorganization (1, 2). The neuronal representation of recently encoded items, for example the reactivation of place cells after behavioral performance, can be demonstrated during high-frequency ripple oscillations (~120–250 Hz) (2–4), which co-occur with sharp waves, a large-amplitude, low-frequency (<10 Hz) signature in the LFP of the hippocampal CA1 region (sharp wave-ripples, SWRs) (5, 6). A contribution of SWRs to memory consolidation is also supported by studies showing that ripples were enhanced posttraining in rats (7–9) and after successful learning in humans (10). In turn, spatial memory tasks followed by the selective disruption of ripples resulted in impaired learning (11–13). However, despite the potentially central role of ripples in memory formation, underlying synaptic mechanisms have not been comprehensively deciphered so far.

As a key mechanism of network oscillations, synaptic inhibition mediated by GABAergic interneurons has been placed at center stage. Both in vivo and in vitro, inhibitory interneurons are able to synchronize the activity of populations of target interneurons and/or principal cells (14–18). Furthermore, certain classes of interneurons are preferentially activated at distinct phases of hippocampal oscillations (19–26), suggesting "division of labor" among GABAergic cells in their contribution to oscillogenesis. Specifically, during SWRs, mainly parvalbumin containing "basket" and "bistratified" neurons are active (20, 21, 27), whereas other types of interneuron are only weakly coupled or silent (20, 23, 28, 29).

Within the neuronal network of the hippocampus, oriens-lacunosum-moleculare (O-LM) interneurons have a peculiar anatomical arrangement with respect to their somatic location and axonal projection area (30–36). At distal apical dendrites of CA1 pyramidal cells, the axonal ramification of O-LM cells overlaps with the termination area of fibers from thalamus and entorhinal cortex, suggesting modulation of input from these brain regions (37–39). Excitatory input onto O-LM cells is primarily local (40), and we wondered about the possibility of sub- and suprathreshold activation of these cells during SWRs. So far, however, synaptic activation onto O-LM interneurons during ripples has not been studied.

Here, we investigated, in a targeted way, activation and activity of cells of interest (41). In particular, we focused on O-LM neurons and studied postsynaptic currents as well as their spiking behavior during SWRs.

Results

We recorded from O-LM interneurons in area CA1 of the hippocampus using both cell-attached and whole-cell patch-clamp techniques. Visually identified by use of infrared-differential interference contrast video microscopy, the somata of these cells were found in stratum oriens and they typically appeared as ovaloids whose longer axis extended in parallel with the pyramidal cell layer. O-LM neurons fulfilled the following criteria: (*i*) axonal ramification in stratum lacunosum-moleculare as identified with post hoc staining, (*ii*) saw-tooth like firing pattern upon mild depolarization, and (*iii*) pronounced voltage sag following hyperpolarization (Fig. 1*A*). In the vicinity of O-LM cells (≤146 μm electrode tip distance), we simultaneously recorded the LFP in the stratum pyramidale (Fig. 1*B*). As described previously (41, 42), ongoing SWR activity in vitro is composed of high-frequency ripples (~120–250 Hz) associated with lower-frequency (<~10 Hz) sharp waves. Spectral analysis revealed a distinct peak at about 200 Hz, indicating ripples (Fig. 1*C*). In voltage-clamp recordings, we observed that O-LM neurons regularly received compound postsynaptic currents (cPSCs) associated with LFP ripples (Fig. 1*B*).

SWR-Associated Synaptic Input onto O-LM Neurons. To characterize contributions of excitatory and inhibitory input onto O-LM neurons during SWRs, we compared this input with the input in pyramidal neurons (41, 43–48) (*SI Materials and Methods, Data Analysis* and Fig. S1). We chose an intermediate holding potential for both cell types (~−60 mV), which allowed us to simultaneously study excitatory and inhibitory contributions (Fig. 1 *D* and *E*). Whereas principal cells displayed a mixed, preferentially outward (inhibitory) current during ripples, O-LM neurons revealed a preponderance of inward currents, indicating stronger excitatory input. For direct comparison, we pooled data from seven O-LM and seven

Author contributions: M.P., N.M., and D.S. designed research; M.P., J.R.D., J.W., A.R.Z., and N.M. performed research; M.P., J.R.D., R.K., and N.M. analyzed data; and M.P., J.R.D., R.K., N.M., and D.S. wrote the paper.

The authors declare no conflict of interest.

*This Direct Submission article had a prearranged editor.

[1]N.M. and D.S. contributed equally to this work.

[2]To whom correspondence may be addressed. E-mail: nikolaus.maier@charite.de or dietmar.schmitz@charite.de.

This article contains supporting information online at www.pnas.org/lookup/suppl/doi:10.1073/pnas.1215496110/-/DCSupplemental.

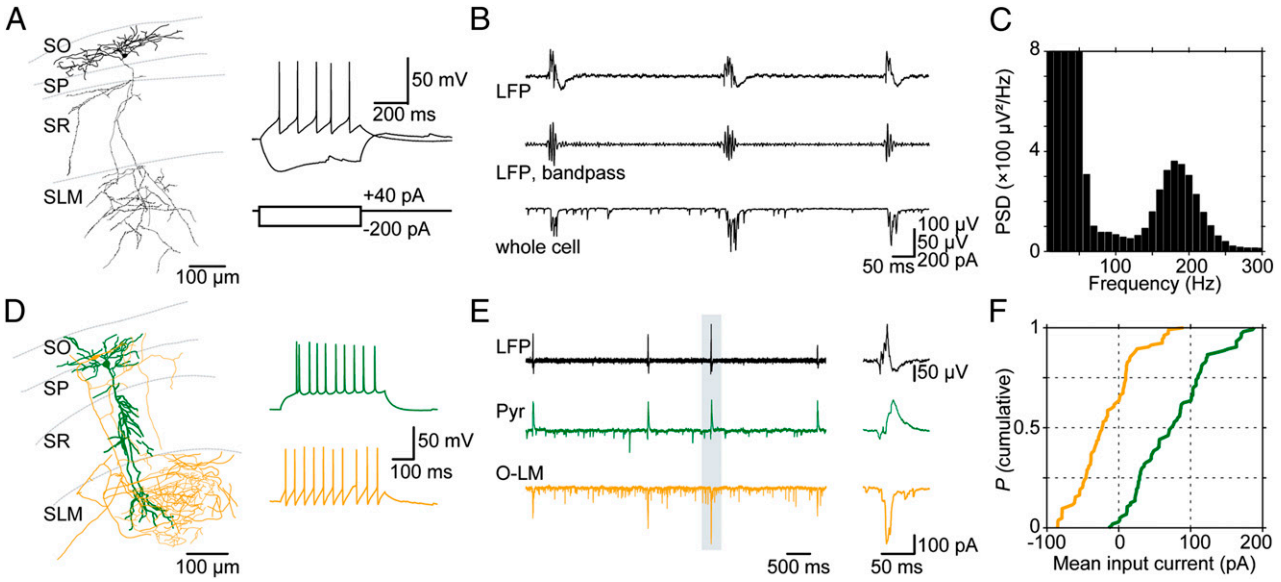

Fig. 1. Ripple-associated synaptic input onto O-LM and pyramidal neurons. (*A*) Reconstruction of an O-LM neuron recorded in area CA1. (*Right*) Electrophysiological characterization of the depicted neuron; note the characteristic "sag potential" in response to hyperpolarization and the typical "saw-tooth" shape of action-potential afterhyperpolarizations. De- and hyperpolarizing current steps as indicated. SO: stratum oriens; SP: stratum pyramidale; SR: stratum radiatum; SLM: stratum lacunosum-moleculare. (*B*) Local field potential (LFP) recording in area CA1 demonstrating spontaneous occurrence of sharp waves (*Top*) and associated ripples (*Middle*, 127–300 Hz bandpass-filtered version of the above). (*Bottom*) Voltage-clamp recording of an O-LM neuron (~–60 mV) demonstrating compound postsynaptic currents associated with SWRs. (*C*) Power spectral density (PSD) of 57 LFP events from the recording presented in *B*; frequency bin width: 10 Hz. Note the peak at ~200 Hz indicating ripple frequency in the LFP signal. (*D Left*) Reconstruction of an O-LM neuron (orange) and a principal cell (green) in area CA1 from a parallel recording. (*Right*) Discharge patterns of the displayed cells. (*E*) Simultaneous LFP and whole-cell voltage-clamp recordings at a slightly depolarized potential (~–60 mV) unmasks inhibitory (outward) currents in the pyramidal neuron, whereas currents in the O-LM cell remain largely inward (excitatory). (*Right*) Magnification of the indicated period. (*F*) Population analysis of average synaptic input current in pyramidal and O-LM neurons (15 randomly picked events from seven pyramidal and seven O-LM neurons). On average, O-LM neurons display consistently larger ripple-associated inward currents compared with pyramids ($P = 1.5 \times 10^{-26}$, K–S test). Quartiles for the distribution of input onto O-LM cells (orange): Median: –23.2 pA, P_{25}: –47.6 pA, P_{75}: +9.7 pA; for pyramidal cells (green): Median: +72.8 pA, P_{25}: +28.8 pA, P_{75}: +110.3 pA.

pyramidal cells and found a systematic bias toward excitation in O-LM cells [15 randomly picked events per cell; $P = 1.5 \times 10^{-26}$, Kolmogorov–Smirnov (K–S) test; Fig. 1*F*].

Timing of Synaptic Input and Spikes in O-LM Cells During Ripples. We recently showed that excitatory input onto CA1 principal neurons during ripples is phasic, coherent across cells, and phase-locked to the LFP (48). To similarly characterize the compound excitatory postsynaptic currents (cEPSCs) onto O-LM neurons, we collected cEPSCs recorded close to the reversal potential of Cl^- (−74 mV; Fig. S2) and derived their corresponding conductances (*SI Materials and Methods, Data Analysis* and Fig. S3). Simultaneous recordings of voltage-clamp signals and the LFP allowed us to compare the timing of excitatory input relative to ripples. First, we juxtaposed the envelopes of conductances and LFPs in the ripple band (127–300 Hz; Fig. 2*A*). Across recordings, the peak of excitatory input sampled from O-LM neurons lagged 3.3 ± 0.3 ms behind the peak of the LFP ($n = 27$ parallel O-LM cell and LFP recordings, 1,791 events analyzed in total; Fig. 2*B*). In addition, we determined the phase-coupling of excitatory input relative to ripple cycles. Across cells, phases ranged between 152° and 284°. Input-to-ripple phase was 209 ± 6° on average, demonstrating robust phase coupling to the ascending part of ripple oscillations (Fig. 2*C*). Similarly, in 18 cells recorded in the current-clamp configuration at resting membrane potential, we observed a coherence peak at ~200 Hz, indicating phase-coupling of ripple-associated postsynaptic potentials and the LFP oscillation (Fig. S4 *A* and *B*).

Previous reports have used intracellular blockers of Cl^--mediated inhibition to investigate excitatory network input at the single-cell level (48, 49). We applied this tool to corroborate the excitatory nature of ripple-locked currents in O-LM neurons. In five repatch–experiments with pharmacologically isolated, stimulus-induced IPSCs, we first verified that perfusion of O-LM cells with the Cl^--channel blocker disodium 4,4′-diisothiocyanatostilbene-2,2′-disulfonate (DIDS; intracellularly applied as CsF-DIDS) significantly reduced inhibition (IPSC reduction to 13.1 ± 3.6% of control; $P = 0.008$, rank-sum test). Having established the efficacy of intracellular CsF-DIDS application, we compared SWR-associated currents without and after perfusion of O-LM neurons with CsF-DIDS (seven repatch experiments with CsF-DIDS application longer than 10 min). In either condition, cEPSC phases were locked to LFP ripples (ranges: 158–223° in control and 157–301° in CsF-DIDS), demonstrating phasic excitatory input (Fig. S5).

Having established ripple-coupled excitatory currents, we asked whether this input is sufficient to recruit O-LM cells into the spiking network. Perfusion of neurons with the patch-pipette solution during whole-cell recordings changes the intracellular milieu, which might lead to alteration of the cell's firing properties. We therefore checked in the noninvasive cell-attached recording configuration whether O-LM neurons expressed spikes. In accord with ripple-locked excitatory input, we identified spiking in 13 of 22 experiments (*Materials and Methods*). Spikes arrived delayed after the ripple maximum (Fig. 3*A*), with a peak spike probability at 6.5 ms (SD: 5.7 ms; *SI Materials and Methods, Data Analysis*; 569 spikes; Fig. 3*B*). Action currents showed a preference for the ascending phase of ripple cycles (mean phase: 219 ± 9°; 350 spikes; 13 cells; range: 173° to 267°; Fig. 3*C*). In a subset of experiments, we found comparable results also for current-clamp recordings (Fig. S4). Collectively, these data demonstrate that ripple-locked excitatory input is sufficient to drive suprathreshold activity in O-LM neurons and spikes are tightly coupled with ripple cycles.

Network Activation Level Determines Spiking in O-LM Neurons. Although all sampled O-LM cells received synaptic input, we identified spiking only in ~59% of recorded neurons (13 of 22 cell-

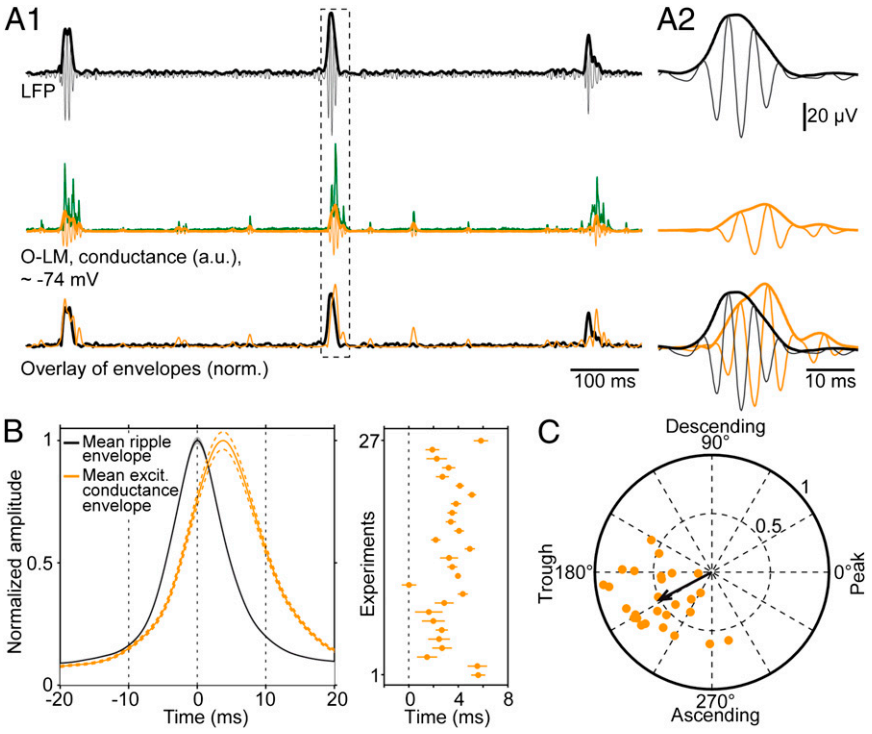

Fig. 2. Synaptic input onto O-LM cells is coherent with ripples. (*A*) Illustration of the analysis. (*A1*) (*Top*) Ripple (127–300 Hz bandpass-filtered LFP, black) overlaid with the envelope (black, bold) derived from the Hilbert transform. (*Middle*) Input conductance (green), its bandpass-filtered version (orange) and the corresponding Hilbert envelope (orange, bold). (*Bottom*) Overlay of normalized envelopes of LFP and excitatory conductances. (*A2*) Magnification of the highlighted period. (*B Left*) Average envelopes of ripples (black) and excitatory conductances (orange) of 27 cells. The average excitatory input conductance in O-LM neurons lags behind the field ripples by 3.3 ± 0.3 ms. (*Right*) The orange dots represent the time points of conductance envelope peaks for all 27 cells (range: 0 ms to 5.8 ms). (*C*) Phases of excitatory conductances with respect to LFP ripples for 27 O-LM cells; orange dots represent the strength and phase of single-cell vectors (black circles and numbers, vector strength scaling; average vector: 208° with a vector strength of 0.51). Across cells, the analysis reveals a strong locking to early ascending ripple phases (mean phase estimation error: 27.1 ± 1.5°; *SI Materials and Methods, Data Analysis*).

attached experiments). We asked whether differences in intrinsic cellular properties could account for this disparity. Neither resting membrane potential ($P = 0.68$, K–S test), nor firing threshold ($P = 0.98$, K–S test) or input resistance ($P = 0.68$, K–S test) were different in spiking and nonspiking cells (Fig. S6). To further investigate the relation between input currents and spiking, we analyzed O-LM cells separately with respect to spiking (or "active") vs. not spiking (or "silent") behavior during ripples. Indeed, spiking probability, i.e., the fraction of SWRs with spikes for a given cell, was correlated with the average excitatory current magnitude in that cell (at −74 mV; $R = -0.5$, $P = 0.017$; Fig. 4*A*). Close to the inhibitory reversal potential, we found systematically larger cEPSCs for active compared with silent cells (at −74 mV, for spiking and silent cells: −82.7 ± 2.7 pA vs. −41.3 ± 2.1 pA; $P = 1.6 \times 10^{-24}$, K–S test; Fig. 4 *B*, *D*, and *E Left*). In addition, when we compared inputs at slightly depolarized voltages to unmask inhibitory synaptic input (−54 mV holding potential), we found only small outward (inhibitory) components in discharging cells in contrast to silent O-LM neurons (Fig. 4*E Right*). Fig. 4*C* summarizes the result for −54 mV holding potential, indicating consistently smaller inward (excitatory) currents with an additional outward current contribution in nonspiking O-LM cells (for spiking and silent cells: −52.4 ± 2.2 pA vs. −8.7 ± 2.5 pA; $P = 4.1 \times 10^{-33}$, K–S test). Together, these data demonstrate overall larger excitatory input in spiking O-LM neurons during ripples and more pronounced inhibitory input in silent cells.

Discussion

Here, we report on two major findings: First, O-LM interneurons consistently receive ripple-associated phasic synaptic input; this input comprises strong excitation, and the ratio of excitation to inhibition in O-LM cells is larger than in CA1 principal cells. Ripple-associated excitation in O-LM neurons lags the LFP ripple by several milliseconds and is phase-locked with field ripples. Second, we observed the suprathreshold recruitment of O-LM cells in 13 out of 22 recordings. Spikes occurred delayed by several milliseconds with respect to the peak of ripples, and they were oscillation-coherent with a preference for the ascending ripple phase.

Our finding of ripple-associated recruitment of O-LM cells is in strong contrast to the previously held view that O-LM neurons exhibit an abrupt drop of spiking during SWRs (20); however, this previous study was conducted on animals anesthetized with urethane and ketamine. By contrast, a recent study on head-fixed, nonanesthetized mice (50) and a second report on freely moving rats (51) demonstrated activation of O-LM cells during SWRs, in line with our in vitro results. In addition to these reports, our data unveil mechanisms that underlie ripple-coherent postsynaptic currents/potentials in the recruitment of O-LM interneurons. To elucidate determinants for spiking and inactivity in O-LM cells, we performed a battery of analyses: Spiking probability was correlated with the magnitude of the respective excitatory input, and the magnitude of excitation was larger in activated vs. silent cells. As factors for active participation, we ruled out resting membrane potential, action potential threshold, and input resistance, i.e., intrinsic cellular properties (Fig. S6). In addition, across cells, we found that the input magnitude and the probability of recruitment were independent of the cell depth below the slice surface, arguing against differences in the amount of severed inputs to influence recruitment (Fig. S7). However, for slices in which O-LM neurons exhibited action potentials during ripples, ripple amplitude, as well

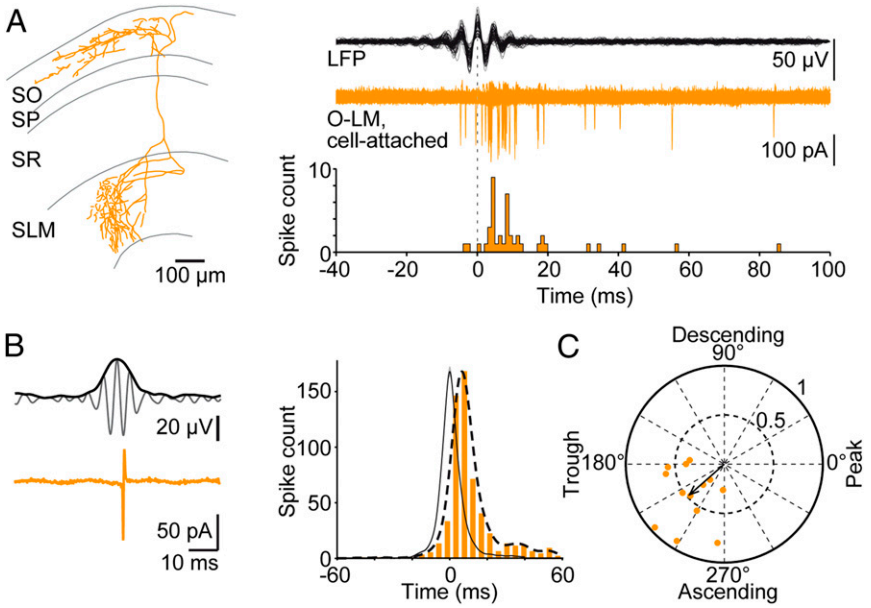

Fig. 3. O-LM cells discharge during SWRs, and spikes are phase-locked to ripple oscillation cycles. (*A Left*) Reconstruction of an O-LM neuron. (*Right*) Overlaid traces of 87 bandpass-filtered (127–300 Hz) ripple episodes (*Top*, black) and respective cell-attached signals recorded from the displayed neuron (*Middle*, orange); all traces were aligned to the ripple maximum (dotted line). (*Bottom*) Spike time histogram of action-currents demonstrating delayed activation of the cell and ripple-locked discharge. (*B Upper Left*) The 127–300 Hz bandpass-filtered LFP overlaid with its envelope. (*Lower Left*) Simultaneously recorded action-currents from the recording shown in *A*. (*Right*) The spike-time histogram (orange) includes all action currents obtained from 13 cell-attached recordings with respect to the peak of each corresponding ripple envelope (average, solid black line; arbitrary units). Overlaid histogram profile (dashed line) represents the sum of Gaussians (σ =3.7 ms) centered on the spike times. Spikes occur late during ripples. (*C*) Polar phase plot indicating average firing phases for the 13 cells recorded in the cell-attached mode (single-cell phase vector tips and vector strength, orange dots); the arrow represents the average vector (221° with a vector strength of 0.47). Note that spike phases cluster to the early ascending phase of ripples.

as the peak amplitude and incidence of sharp waves were enhanced, suggesting an influence of levels of excitability (Fig. S8). Finally, ripple-accompanied inhibition was more pronounced for nonspiking vs. discharging cells. In sum, all these findings advocate that the magnitude of excitatory network activity and the ratio of excitatory and inhibitory input determine whether O-LM cells are recruited into the active network.

The maximum of ripple-locked excitation and the peak of O-LM cell spiking probability lagged the field ripple by several milliseconds. Two lines of explanation are feasible: First, even though CA1 principal cells discharge at low firing rates during ripples (47), their activity might be sufficient to explain ripple-locked input into an O-LM neuron if an assembly of sparsely spiking pyramidal cells projects to the O-LM neuron and if the assembly's output is modulated by GABAergic interneurons (17, 52). In particular, axo-axonic cells, which target the axon initial segment of principal neurons (35, 53), have their peak firing probability early during ripples and are silent after the ripple maximum (20). This behavior might account for the delayed recruitment of O-LM cells during ripples. Second, as shown recently for gamma oscillations in area CA3, pyramidal cell axon spiking outnumbers firing observed at the level of the soma (54). This experimental observation might also be applicable to ripples in area CA1, an assumption that is supported by modeling results suggesting a network of coupled axons as the origin of ripples (47, 55–57). In this framework, the output of the axonal network might represent the source of field-ripple-coherent excitatory input onto O-LM interneurons. In agreement with this hypothesis, the delayed arrival of input could also be explained by synaptic facilitation, a well known property of excitatory synapses onto O-LM cells in area CA1 (30, 33, 58–60). Specifically, these connections have a low initial release probability and therefore express robust short-term facilitation that might be regulated by neuromodulation (30). In support, presynaptic glutamatergic terminals targeting onto O-LM neurons are highly equipped with metabotropic glutamate receptors (20, 58, 61). In either of the above-mentioned scenarios, the delay of synaptic input and late discharge of O-LM cells could be accounted for. Moreover, the delayed discharge of O-LM cells could likewise be the result of temporal summation of synaptic input.

In area CA1, a consequence of O-LM cell recruitment during SWRs could be the gating of cortical vs. CA3 input. In support, Leão et al. (62) have recently shown that O-LM cell activity can boost Schaffer collateral over entorhinal input in CA1 by inhibition of interneurons in stratum radiatum. By contrast, O-LM cell activation could suppress temporoammonic feed-forward inhibition resulting in accentuation of the excitatory component of entorhinal input (39, 63). Alternatively, O-LM cell-mediated monosynaptic inhibition at distal apical dendrites of CA1 principal cells might hyperpolarize these neurons even at the somatic level (35), thereby reducing their excitability. In any case, in area CA1 the modulation of activity of O-LM neurons during SWRs would serve an important strategic role in routing CA3 vs. entorhinal input during wakeful quiescence or slow-wave sleep.

In summary, we have demonstrated reliable subthreshold activation of O-LM neurons during ripples and the input-dependent suprathreshold recruitment of these cells into the active network. Our findings point to a previously uncharacterized role of O-LM neurons with respect to modulation of ripple-correlated input from entorhinal afferents into CA1. Future work will have to define the behavioral consequences of ripple-associated recruitment of O-LM cells, or their inactivity.

Materials and Methods

Animal husbandry was done in accordance with the German animal welfare act and the Directive 2010/63/EU of the European Parliament and of the Council of 22 September 2010 on the protection of animals used for scientific purposes. Experiments and animal maintenance were in accordance with the guidelines of the Berlin state authorities (T0100/03).

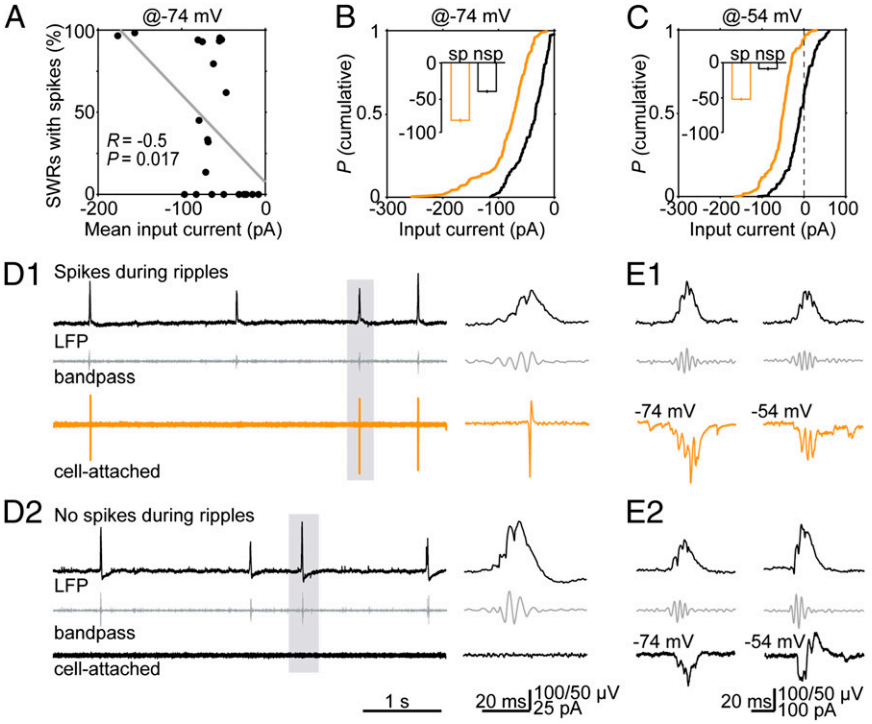

Fig. 4. The magnitude of input currents determines the recruitment of O-LM neurons during ripples. (*A*) The spiking probability of O-LM cells during SWRs is correlated to their mean input current ($R = -0.5$; $P = 0.017$; $n = 22$ experiments). (*B*) Cumulative probability of the average input current in O-LM cells held at −74 mV for spiking (orange) and silent cells (black). Quartiles of spiking cells: Median: −72.9 pA, P_{25}: −93.8 pA, P_{75}: −53.7 pA; quartiles of nonspiking cells: Median: −33.8 pA, P_{25}: −59.1 pA, P_{75}: −19.3 pA. (*Inset*) The mean values (sp: spiking; nsp: nonspiking or silent). (*C*) Distributions of average input currents for spiking (orange) and silent (black) O-LM neurons held at −54 mV. Quartiles of spiking cells: Median: −49.2 pA, P_{25}: −66.6 pA, P_{75}: −33.5 pA; quartiles of nonspiking cells: Median: −8.2 pA, P_{25}: −27.4 pA, P_{75}: 12.1 pA. The inset shows the means values. (*D Upper*) Unfiltered LFP. (*Middle*) 127–300 Hz bandpass-filtered LFP. (*Lower*) Cell-attached recording of a spiking (*Upper*, D1, orange) and of a nonspiking O-LM cell (*Lower*, D2, black). (*Right*) Magnifications of the highlighted events. (*E Top*) Unfiltered LFP. (*Middle*) Bandpass-filtered LFP. (*Bottom*) cPSCs of a spiking (E1, orange) and a nonspiking O-LM cell (E2, black) close to the reversal potential of Cl^- (−74 mV, *Left*) and at −54 mV (*Right*).

Experimental Procedures; Slice Preparation. C57BL/6 mice of age 3–6 wk were either decapitated or decapitated following isoflurane anesthesia. Brains were transferred to standard artificial cerebrospinal fluid (1–4 °C) containing 119 mM NaCl, 2.5 mM KCl, 1.3 mM $MgCl_2$, 2.5 mM $CaCl_2$, 10 mM glucose, 1.0 mM NaH_2PO_4, and 26 mM $NaHCO_3$, enriched with carbogen [95% (vol/vol) O_2/5% (vol/vol) CO_2; pH 7.4 at 37 °C; 290–310 mosmol/L]. Horizontal slices (400 µm) of ventral to midhippocampus were cut on a slicer (VT1200S; Leica) and stored in an interface chamber [32–34 °C, continuously oxygenized with carbogen, and perfused with artificial cerebrospinal fluid (ACSF) at ∼1 mL/min]. Slices were allowed to recover for at least 1.5 h after preparation.

Electrophysiology. As described (41), recordings were performed in standard ACSF at 31–32 °C in a submerged-type recording chamber perfused at high rate (5–6 mL/min). For LFP recordings, glass microelectrodes (tip diameter ∼5–10 µm; resistance: 0.2–0.3 MΩ) were filled with ACSF before use. LFP signals in the CA1 pyramidal cell layer were amplified 1,000-fold, filtered (1–8 kHz), and sampled at 5 or 20 kHz. Whole-cell and extracellular recordings were performed using a Multiclamp 700A amplifier (Axon Instruments). For parallel cell-and-field recordings, a custom-made two-channel extracellular amplifier was used. Whole-cell recordings were performed with borosilicate glass electrodes (2–5 MΩ) filled with 120 mM K-gluconate, 10 mM Hepes, 3 mM Mg-ATP, 10 mM KCl, 5 mM EGTA, 2 mM $MgSO_4$, 0.3 mM Na-GTP, and 14 mM phosphocreatine. For a subset of experiments (Fig. 1 *D–F*) another solution was used: 135 mM K-gluconate, 10 mM Hepes, 2 mM Mg-ATP, 20 mM KCl, 0.2 mM EGTA. The pH of these intracellular solutions was adjusted to 7.4 with KOH. To block chloride currents intracellularly, we chose a CsF-DIDS-based solution: 120 mM Cs-fluoride, 10 mM KCl, 10 mM Hepes, 5 mM EGTA, and 1 mM disodium 4,4′-diisothiocyanatostilbene-2,2′-disulfonate (DIDS); pH adjusted to 7.4 with NaOH.

Cell Identification. Horizontal cells with fusiform somata were identified using infrared differential interference contrast (IR-DIC) video microscopy. Depth of cells was ≥50 µm below the slice surface (range: 50–127 µm; median: 65 µm; 37 cells; see also Fig. S7). Before rupturing the cell membrane, cells were kept in the cell-attached configuration to record action currents, if present. Later analysis of cell-attached data included only experiments with periods ≥60 s in this recording condition. In the whole-cell configuration, de- and hyperpolarizing current steps (800–1,000 ms) were applied to characterize the cell's intrinsic properties; only cells that showed typical spiking characteristics of O-LM neurons (see below) or principal cells ("regular" discharge pattern, low or no sag potential) were considered. The series resistance, R_s, was monitored continuously throughout experiments, and data were rejected if R_s was >25 MΩ or varied more than ±30% during recordings. R_s compensation was not used. All indicated cellular potentials are liquid junction potential-corrected (calculated ∼14 mV, experimentally verified). The reversal potential of chloride was experimentally determined revealing ∼ −67 mV for pyramidal cells and ∼ −76.8 mV for O-LM cells (Fig. S2).

Applied Drugs. D-(-)-2-Amino-5-phosphonopentanoic acid (D-APV), 6-Imino-3-(4-methoxyphenyl)-1(6H)-pyridazinebutanoic acid hydrobromide (gabazine), and (2S)-(+)-5,5-Dimethyl-2-morpholinea cetic acid (SCH50911) were obtained from Biotrend. 2,3-dioxo-6-nitro-1,2,3,4-tetrahydrobenzo(f)quinoxaline-7-sulfonamide (NBQX), disodium 4,4′-diisothiocyanatostilbene-2,2′-disulfonate (DIDS), and cesium fluoride were purchased from Sigma Aldrich.

A detailed layout of the procedures applied for data analyses are provided in *SI Materials and Methods*.

ACKNOWLEDGMENTS. We thank Susanne Rieckmann and Anke Schönherr for their continuous, excellent technical assistance, and Christian Wozny, Genela Morris, and Sarah Shoichet for comments on the manuscript. This study was supported by Deutsche Forschungsgemeinschaft (SFB 618 and SFB 665) and Bundesministerium für Bildung und Forschung (Grants 01GQ1001A and 01GQ0972, Exc 257, and Deutsches Zentum für Neurodegenerative Erkrankungen, DZNE).

1. Wilson MA, McNaughton BL (1994) Reactivation of hippocampal ensemble memories during sleep. *Science* 265(5172):676–679.
2. Lee AK, Wilson MA (2002) Memory of sequential experience in the hippocampus during slow wave sleep. *Neuron* 36(6):1183–1194.
3. Diba K, Buzsáki G (2007) Forward and reverse hippocampal place-cell sequences during ripples. *Nat Neurosci* 10(10):1241–1242.
4. O'Neill J, Senior TJ, Allen K, Huxter JR, Csicsvari J (2008) Reactivation of experience-dependent cell assembly patterns in the hippocampus. *Nat Neurosci* 11(2):209–215.
5. Buzsáki G (1986) Hippocampal sharp waves: Their origin and significance. *Brain Res* 398(2):242–252.
6. Buzsáki G, Horváth Z, Urioste R, Hetke J, Wise K (1992) High-frequency network oscillation in the hippocampus. *Science* 256(5059):1025–1027.
7. Ponomarenko AA, Li JS, Korotkova TM, Huston JP, Haas HL (2008) Frequency of network synchronization in the hippocampus marks learning. *Eur J Neurosci* 27(11): 3035–3042.
8. Eschenko O, Ramadan W, Mölle M, Born J, Sara SJ (2008) Sustained increase in hippocampal sharp-wave ripple activity during slow-wave sleep after learning. *Learn Mem* 15(4):222–228.
9. Ramadan W, Eschenko O, Sara SJ (2009) Hippocampal sharp wave/ripples during sleep for consolidation of associative memory. *PLoS ONE* 4(8):e6697.
10. Axmacher N, Elger CE, Fell J (2008) Ripples in the medial temporal lobe are relevant for human memory consolidation. *Brain* 131(Pt 7):1806–1817.
11. Ego-Stengel V, Wilson MA (2010) Disruption of ripple-associated hippocampal activity during rest impairs spatial learning in the rat. *Hippocampus* 20(1):1–10.
12. Girardeau G, Benchenane K, Wiener SI, Buzsáki G, Zugaro MB (2009) Selective suppression of hippocampal ripples impairs spatial memory. *Nat Neurosci* 12(10): 1222–1223.
13. Jadhav SP, Kemere C, German PW, Frank LM (2012) Awake hippocampal sharp-wave ripples support spatial memory. *Science* 336(6087):1454–1458.
14. Cobb SR, Buhl EH, Halasy K, Paulsen O, Somogyi P (1995) Synchronization of neuronal activity in hippocampus by individual GABAergic interneurons. *Nature* 378(6552): 75–78.
15. Tamás G, Buhl EH, Lörincz A, Somogyi P (2000) Proximally targeted GABAergic synapses and gap junctions synchronize cortical interneurons. *Nat Neurosci* 3(4):366–371.
16. Bartos M, et al. (2002) Fast synaptic inhibition promotes synchronized gamma oscillations in hippocampal interneuron networks. *Proc Natl Acad Sci USA* 99(20): 13222–13227.
17. Brunel N, Wang XJ (2003) What determines the frequency of fast network oscillations with irregular neural discharges? I. Synaptic dynamics and excitation-inhibition balance. *J Neurophysiol* 90(1):415–430.
18. Royer S, et al. (2012) Control of timing, rate and bursts of hippocampal place cells by dendritic and somatic inhibition. *Nat Neurosci* 15(5):769–775.
19. Csicsvari J, Hirase H, Czurkó A, Mamiya A, Buzsáki G (1999) Oscillatory coupling of hippocampal pyramidal cells and interneurons in the behaving Rat. *J Neurosci* 19(1): 274–287.
20. Klausberger T, et al. (2003) Brain-state- and cell-type-specific firing of hippocampal interneurons in vivo. *Nature* 421(6925):844–848.
21. Klausberger T, et al. (2004) Spike timing of dendrite-targeting bistratified cells during hippocampal network oscillations in vivo. *Nat Neurosci* 7(1):41–47.
22. Hájos N, et al. (2004) Spike timing of distinct types of GABAergic interneuron during hippocampal gamma oscillations in vitro. *J Neurosci* 24(41):9127–9137.
23. Klausberger T, et al. (2005) Complementary roles of cholecystokinin- and parvalbumin-expressing GABAergic neurons in hippocampal network oscillations. *J Neurosci* 25(42):9782–9793.
24. Oren I, Mann EO, Paulsen O, Hájos N (2006) Synaptic currents in anatomically identified CA3 neurons during hippocampal gamma oscillations in vitro. *J Neurosci* 26(39): 9923–9934.
25. Wulff P, et al. (2009) Hippocampal theta rhythm and its coupling with gamma oscillations require fast inhibition onto parvalbumin-positive interneurons. *Proc Natl Acad Sci USA* 106(9):3561–3566.
26. Gulyás AI, et al. (2010) Parvalbumin-containing fast-spiking basket cells generate the field potential oscillations induced by cholinergic receptor activation in the hippocampus. *J Neurosci* 30(45):15134–15145.
27. Lapray D, et al. (2012) Behavior-dependent specialization of identified hippocampal interneurons. *Nat Neurosci* 15:1265–1271.
28. Jinno S, et al. (2007) Neuronal diversity in GABAergic long-range projections from the hippocampus. *J Neurosci* 27(33):8790–8804.
29. Fuentealba P, et al. (2008) Ivy cells: A population of nitric-oxide-producing, slow-spiking GABAergic neurons and their involvement in hippocampal network activity. *Neuron* 57(6):917–929.
30. McBain CJ, DiChiara TJ, Kauer JA (1994) Activation of metabotropic glutamate receptors differentially affects two classes of hippocampal interneurons and potentiates excitatory synaptic transmission. *J Neurosci* 14(7):4433–4445.
31. Sík A, Penttonen M, Ylinen A, Buzsáki G (1995) Hippocampal CA1 interneurons: an in vivo intracellular labeling study. *J Neurosci* 15(10):6651–6665.
32. Maccaferri G, McBain CJ (1996) Long-term potentiation in distinct subtypes of hippocampal nonpyramidal neurons. *J Neurosci* 16(17):5334–5343.
33. Ali AB, Thomson AM (1998) Facilitating pyramid to horizontal oriens-alveus int7rneurone inputs: dual intracellular recordings in slices of rat hippocampus. *J Physiol* 504(Pt 1):185–199.
34. Katona I, Acsády L, Freund TF (1999) Postsynaptic targets of somatostatin-immunoreactive interneurons in the rat hippocampus. *Neuroscience* 88(1):37–55.
35. Maccaferri G, Roberts JD, Szucs P, Cottingham CA, Somogyi P (2000) Cell surface domain specific postsynaptic currents evoked by identified GABAergic neurones in rat hippocampus in vitro. *J Physiol* 524(Pt 1):91–116.
36. Maccaferri G (2005) Stratum oriens horizontal interneurone diversity and hippocampal network dynamics. *J Physiol* 562(Pt 1):73–80.
37. Wouterlood FG, Saldana E, Witter MP (1990) Projection from the nucleus reuniens thalami to the hippocampal region: Light and electron microscopic tracing study in the rat with the anterograde tracer Phaseolus vulgaris-leucoagglutinin. *J Comp Neurol* 296(2):179–203.
38. Colbert CM, Levy WB (1992) Electrophysiological and pharmacological characterization of perforant path synapses in CA1: Mediation by glutamate receptors. *J Neurophysiol* 68(1):1–8.
39. Empson RM, Heinemann U (1995) The perforant path projection to hippocampal area CA1 in the rat hippocampal-entorhinal cortex combined slice. *J Physiol* 484(Pt 3): 707–720.
40. Blasco-Ibáñez JM, Freund TF (1995) Synaptic input of horizontal interneurons in stratum oriens of the hippocampal CA1 subfield: Structural basis of feed-back activation. *Eur J Neurosci* 7(10):2170–2180.
41. Maier N, Morris G, Johenning FW, Schmitz D (2009) An approach for reliably investigating hippocampal sharp wave-ripples in vitro. *PLoS ONE* 4(9):e6925.
42. Maier N, Nimmrich V, Draguhn A (2003) Cellular and network mechanisms underlying spontaneous sharp wave-ripple complexes in mouse hippocampal slices. *J Physiol* 550(Pt 3):873–887.
43. Ylinen A, et al. (1995) Sharp wave-associated high-frequency oscillation (200 Hz) in the intact hippocampus: Network and intracellular mechanisms. *J Neurosci* 15(1 Pt 1): 30–46.
44. Wu C, Shen H, Luk WP, Zhang L (2002) A fundamental oscillatory state of isolated rodent hippocampus. *J Physiol* 540(Pt 2):509–527.
45. Wu CP, et al. (2006) Spontaneous rhythmic field potentials of isolated mouse hippocampal-subicular-entorhinal cortices in vitro. *J Physiol* 576(Pt 2):457–476.
46. Both M, Bähner F, von Bohlen und Halbach O, Draguhn A (2008) Propagation of specific network patterns through the mouse hippocampus. *Hippocampus* 18(9): 899–908.
47. Bähner F, et al. (2011) Cellular correlate of assembly formation in oscillating hippocampal networks in vitro. *Proc Natl Acad Sci USA* 108(35):E607–E616.
48. Maier N, et al. (2011) Coherent phasic excitation during hippocampal ripples. *Neuron* 72(1):137–152.
49. Nelson S, Toth L, Sheth B, Sur M (1994) Orientation selectivity of cortical neurons during intracellular blockade of inhibition. *Science* 265(5173):774–777.
50. Varga C, Golshani P, Soltesz I (2012) Frequency-invariant temporal ordering of interneuronal discharges during hippocampal oscillations in awake mice. *Proc Natl Acad Sci USA* 109(40):E2726–E2734.
51. Katona L, et al. (2012) Behaviourally-defined activity dynamics of GABAergic O-LM interneurons in the rat hippocampus. *FENS Forum Abstr* 1872:F58.
52. Taxidis J, Coombes S, Mason R, Owen MR (2012) Modeling sharp wave-ripple complexes through a CA3-CA1 network model with chemical synapses. *Hippocampus* 22(5):995–1017.
53. Somogyi P, et al. (1985) Identified axo-axonic cells are immunoreactive for GABA in the hippocampus and visual cortex of the cat. *Brain Res* 332(1):143–149.
54. Dugladze T, Schmitz D, Whittington MA, Vida I, Gloveli T (2012) Segregation of axonal and somatic activity during fast network oscillations. *Science* 336(6087): 1458–1461.
55. Traub RD, Schmitz D, Jefferys JG, Draguhn A (1999) High-frequency population oscillations are predicted to occur in hippocampal pyramidal neuronal networks interconnected by axoaxonal gap junctions. *Neuroscience* 92(2):407–426.
56. Traub RD, Schmitz D, Maier N, Whittington MA, Draguhn A (2012) Axonal properties determine somatic firing in a model of in vitro CA1 hippocampal sharp wave/ripples and persistent gamma oscillations. *Eur J Neurosci* 36(5):2650–2660.
57. Draguhn A, Traub RD, Schmitz D, Jefferys JG (1998) Electrical coupling underlies high-frequency oscillations in the hippocampus in vitro. *Nature* 394(6689):189–192.
58. Losonczy A, Zhang L, Shigemoto R, Somogyi P, Nusser Z (2002) Cell type dependence and variability in the short-term plasticity of EPSCs in identified mouse hippocampal interneurones. *J Physiol* 542(Pt 1):193–210.
59. Losonczy A, Somogyi P, Nusser Z (2003) Reduction of excitatory postsynaptic responses by persistently active metabotropic glutamate receptors in the hippocampus. *J Neurophysiol* 89(4):1910–1919.
60. Biró AA, Holderith NB, Nusser Z (2005) Quantal size is independent of the release probability at hippocampal excitatory synapses. *J Neurosci* 25(1):223–232.
61. Shigemoto R, et al. (1996) Target-cell-specific concentration of a metabotropic glutamate receptor in the presynaptic active zone. *Nature* 381(6582):523–525.
62. Leão RN, et al. (2012) OLM interneurons differentially modulate CA3 and entorhinal inputs to hippocampal CA1 neurons. *Nat Neurosci* 15(11):1524–1530.
63. Elfant D, Pál BZ, Emptage N, Capogna M (2008) Specific inhibitory synapses shift the balance from feedforward to feedback inhibition of hippocampal CA1 pyramidal cells. *Eur J Neurosci* 27(1):104–113.